Dept. of Mech. Eng.
CUET

Published Online April 2017 (http://www.cuet.ac.bd/merj/index.html)

Mechanical Engineering Research Journal

Vol. 10, pp. 41-46, 2016

ISSN: 1990-5491

STUDY OF FLUID DYNAMICS APPROACH TO SCALE GROWTH MECHANISM AND ITS SUPPRESSION TECHNIQUE

P. Das[1*], M. M. K. Khan[2], M. G. Rasul[3] and S. C. Saha[4]

[1,2,3]School of Engineering and Technology, Central Queensland University, Australia
[4]School of Chemistry, Physics and Mechanical Engineering, Queensland University of Technology, Australia

Abstract: Scale is probably a more severe problem in the minerals industry than other process industries. It often leads to serious on-going technical problems and is a major cause of production loss due to equipment downtime required for descaling and cleaning operations. Gibbsite scale formation in Bayer process equipment is a natural consequence of supersaturated solutions that are generated throughout the process. The article describes one example applications: the fluid flow characteristics on scale deposition in a concentric reducer using Reynolds stress model are analysed. Reynolds stress simulation method to analyse the fluid dynamics behavior of water as it flows through a concentric reducer commonly used in the Bayer plant is presented. The simulation results show a significant variation of the stream-wise and cross-stream components of the fluctuating velocity as flow passes through the concentric reducer.

Keywords: *Scale growth, Suppression, Bayer process, concentric reducer and Fluctuating velocity components.*

NOMENCLATURE

u_r = cross-stream component of instantaneous velocity (m s^{-1})
$\overline{u}_r$ = time-averaged value of the cross-stream velocity component state transition matrix (m s^{-1})
u_r' = fluctuating component of cross-stream velocity (m s^{-1})
$\sqrt{(u_r')^2}$ = root-mean-square of the fluctuating cross-stream velocity
$\sqrt{(u_x')^2}$ = root-mean-square of the fluctuating stream-wise velocity

1. INTRODUCTION

Scale deposition or precipitation in pipeline and process equipment is intrinsic to the operation of several mineral process industries. Scale formation in the mineral process equipment is a natural consequence of supersaturated solutions that are generated throughout the process. The accumulation of scale reduces the production efficiency considerably and causes other problems such as pipe blockage, probe malfunction, reduction in heat exchanger efficiency and operational costs involved in the de-scaling process. Typical examples of equipment that suffer from scaling are domestic washing machine (Fig. 1(a)), process pipe line (Fig. 1 (b)) and membrane (Fig. 1(c)).

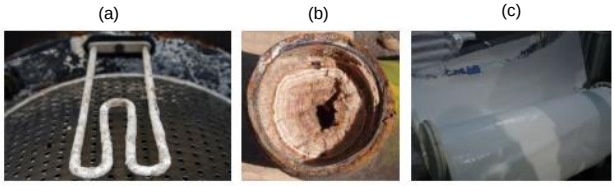

Fig. 1 Typical examples of scaling, (a) domestic: Washing machine, (b) Industrial: Scaling in pipe and (c) Industrial; Scaling on membrane [1].

2. OVERVIEW OF BAYER PROCESS SCALING

The Bayer process cycle is used for extracting bauxite from ore to refining grade alumina (Al_2O_3). The resulting liquor, termed pregnant or green liquor, which is supersaturated in sodium aluminate, is then clarified and filtered to remove mud and other insoluble impurities. After solid impurities separation, gibbsite or $Al(OH)_3$ is precipitated. This is accomplished by cooling the solution and seeding with gibbsite. The extraction process depends completely on chemical processes occurring at the solid/aqueous interface as shown below [2]:

Extraction: $Al(OH)_{3(s)} + NaOH_{(aq)} \rightarrow Na^+ Al(OH)_{4(aq)}^-$

[*] **Corresponding author:** Email: p.das@cqu.edu.au; Tel: +61-469304900; Fax: +61-7 4930 9382

and $AlO(OH)_{(s)} + NaOH_{(aq)} + H_2O \rightarrow Na^+ Al(OH)^-_{4(aq)}$

Precipitation: $Na^+ Al(OH)^-_{4(aq)} \rightarrow Al(OH)_{3(s)} + NaOH_{(aq)}$

Calcination: $2Al(OH)_{3(s)} \rightarrow Al_2O_{3(s)} + 3H_2O_{(g)}$

In the Bayer process, caustic liquors are used to dissolve gibbsite from the bauxite ore at temperatures up to 270 ºC, and then to re-precipitate as a hydrate at low temperature. A consequence of the Bayer process is that the liquors are purposely kept supersaturated with respect to gibbsite and thus scaling occurs as shown in Fig. 2.

The scale deposition in pipeline and process equipment commonly happens in mineral refining processes including such industries as nickel, magnesium and alumina refining [4]. In alumina refineries, the most rapid scale formation occurs in the precipitation area where alumina is chemically extracted from bauxite. The basic scaling mechanisms are of two of types, “growth scale” and “settled scale”.

Growth scale is due to the crystallisation of gibbsite from the supersaturated caustic solution. Nucleation can be a slow process of scale growth and is governed by many factors; however, once the nuclei are formed, growth is very predictable based on kinetic factors such as temperature and supersaturation. The degree of supersaturation and surface condition are very critical factors for nucleation. For example, pipe and tank walls are often cooler than the liquor, hence the local supersaturation at the surface will be higher, and nucleation will be more favourable at that point**.**

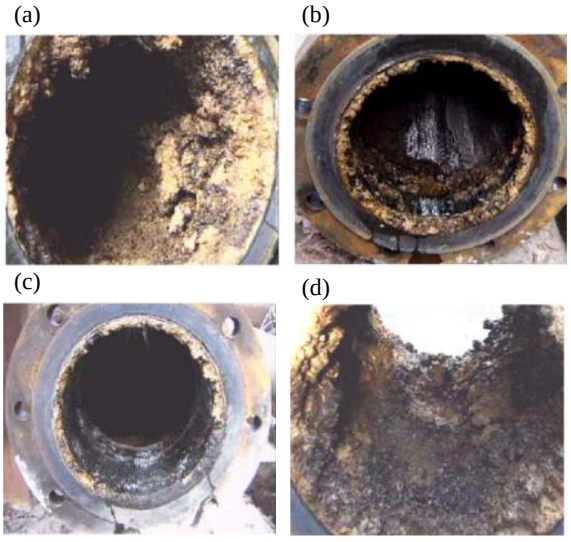

Fig. 2 Gibbsite scale growth observed in components of the test pipe [4].

In the settled scale, the slurry particles may be settled and cemented by the supersaturated liquor. Settling scale occurs more favourably to low velocity regions of plant equipment or during shut downs. Agitation also plays an important role in settling scale. Examples of each scale type can be found in the same slurry, such as in a precipitator and a digest vessel.

3. SCALE GROWTH MECHANISM

The rate-determining stage in the Bayer process cycle is the crystallisation of gibbsite from the supersaturated caustic-aluminate solution. As reported by Watson *et al*. [5], the formation of gibbsite crystals is the most rapid in the temperature range of 60 ºC to 80 ºC due to the balance between supersaturation and reaction kinetics. In an ideal supersaturated caustic-aluminate solution, the dissolution of gibbsite phase aluminate-trihydrate occurs according to the simplified chemical reaction [6]:

$$Al(OH)_{3(s)} + OH^- \Leftrightarrow Na^+ Al(OH)^-_{4(aq)}$$

The observation of Watson *et al.* [5] is that exact mechanism by which the $Al(OH)^-_4$ ions in the supersaturated caustic-aluminate solution nucleate and grow into the crystalline gibbsite is not fully understood. The sequence of settled and crystalized scale formation may be visualized as shown in Fig. 3. Demopoulos [7] reported that super-saturation is the important parameter of crystalized scale formation.

The mathematical analysis of the assumed overall chemical reaction describing the crystallization process may be expressed in the form as [8]:

$$k_r = A_1 e^{-\frac{E}{RT}} \tag{1}$$

The first general model to describe the crystallization fouling process was devised by Kern and Seaton [9], the model has the form

$$R_f = R_{f\infty}\left(1 - e^{\frac{t-t_d}{t_c}}\right) \tag{2}$$

If the induction time is small, the Eq. (2) reverts to

$$R_f = R_{f\infty}\left(1 - e^{-\frac{t}{t_c}}\right) \tag{3}$$

The most of early studies (e.g. [3, 10-13]) have found a decrease in the fouling and scale with increasing fluid velocity. Fahiminia *et al.* [14] examine that calcium sulphate dehydrated (gypsum) scales under sensible heating conditions and measured the influence of fluid velocity and surface temperature, as well as bulk temperature and concentration on precipitation fouling induction period. The induction period decreased with increasing bulk solute concentration and surface temperature, and decreased with increasing fluid velocity [3].

Amjad [15] studied gypsum deposition on various metal surfaces and reported that scale formation is a function of surface area and the metallurgy of the heat exchanger. Yang *et al.* [16] investigated copper and copper-modified, low-energy surface SAM and reported that the nucleation rate on a low-energy surface is lower than that on a high energy surface.

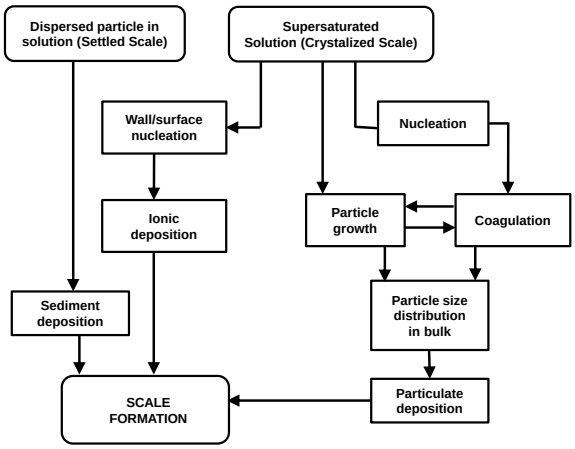

Fig. 3 Mechanism of scale formation.

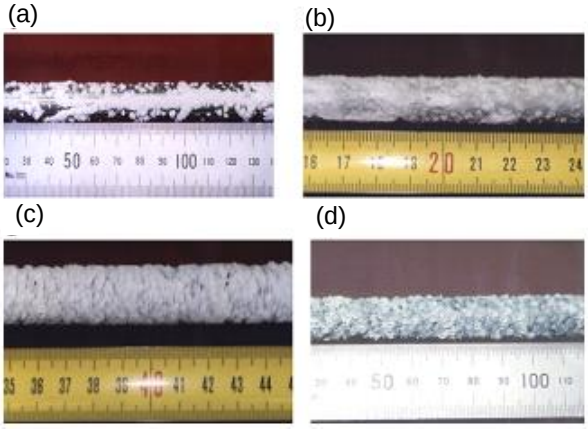

Fig. 4 Deposition on smooth SS 316 (a), aluminium (b), brass (c) and copper (d) surfaces. ΔT 15ºC, bulk temperature 40ºC, solution conc. 3.6 g/L, 4000 min [18].

Tianqing *et al.* [17] observed that both the nucleating and growth rates of calcium carbonate particles on heated surface increase rapidly with the concentration solutions. Kazi *et al.* [18, 19] investigated mineral scale formation and mitigation on different heat exchanger surface as shown in Fig. 4. It is reported that scaling on different metal surfaces increases with increasing thermal conductivity and surface roughness (cooper>aluminium>brass>stainless steel).

4. SCALE SUPPRESSION APPROACH

A novel scale-velocity model was developed [13] for elucidation the scale growth and suppression in an alumina refinery. In this model, a relationship between the fluid flow velocity and scale formation is schematically illustrated in Fig. 5 [13]. There are four regimes recognized to understand the scale growth mechanism, namely regimes (A) mass transfer control, (B) chemical reaction control, (C) suppression by erosion and (D) erosion damage. The following subsections discuss about important regimes are (C) and (D).

In regime C, the rate of scale growth progressively decreases with increase in fluid velocity. In this regime, an increase in fluid velocity results in more erosion, which slows down the scale growth [13]. Measurements of scale growth were examined in a series of different diameter pipes connected through the fittings, and concluded that scales growth decreases with increasing slurry velocity in the range from 0.5 to 1.7 m/s as shown in Fig. 6.

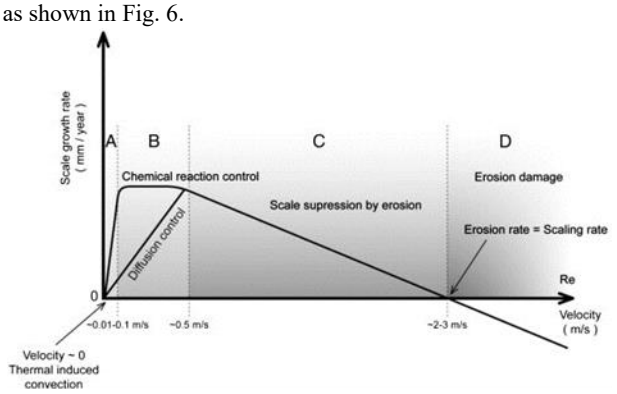

Fig. 5 Relationship between the precipitation or chemical reaction driven scale growth rate and fluid velocity [13].

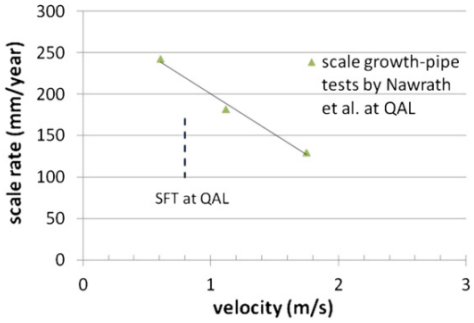

Fig. 6 Scale growth rate corresponding fluid velocity based on tests using pipes in the precipitation area at QAL [4].

In regime D, the material surface suffers net loss owing to the effect of erosion more than scale growth. Wu *et al.* [13] concluded that regimes C and D are more significant for scale suppression in terms of fluid dynamics design strategy [13]. They developed a new precipitation tank design with swirl flow technology (SFT) as shown in Fig. 7.

Stegink *et al.*, [20] reported that this design doubles the service life between de-scaling operations with SFT design as compared to the conventional draft tube design. SFT agitation at QAL was designed mainly based on fluid dynamics point of view. It has been long established that the tangential velocity near the wall boundary surface plays a critical role on suppression of scale growth. The non-dimensional velocity efficiency parameter (η), $\eta = V/(P/\rho A)^{1/3}$ along the tank height was examined by CFD simulation [13] as shown in Fig. 8.

Another approach of material removal from a solid surface by cavitation associated with the formation and collapse of bubbles. Cavitation is the phenomena of the rapid formation and implosion of bubbles in an area of low-pressure in liquids by means of mechanical forces. Fig. 9 gives an overview of ultrasonic cavitation.

Ashley [22] studied preventing of potassium nitrate scale on a heat exchange surface by using sonification. Fig. 10 shows the experimental setup for crystallizing potassium nitrate, both

with and without ultrasound. It is reported that ultrasonically activating coil prevents the encrustation on cooling coil.

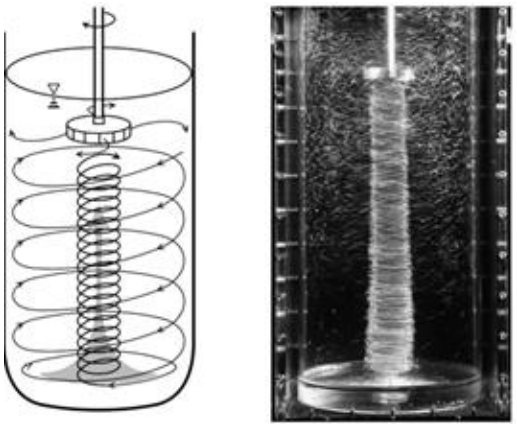

Fig. 7 Swirl flow technology, showing the intense inner vortex and high wall velocities [13].

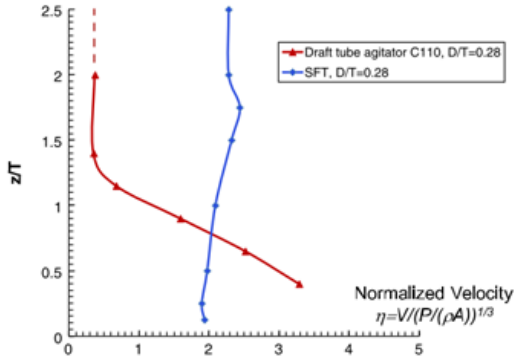

Fig. 8 Non-dimension velocity efficiency parameter profile along the tank height, measured near the wall [13].

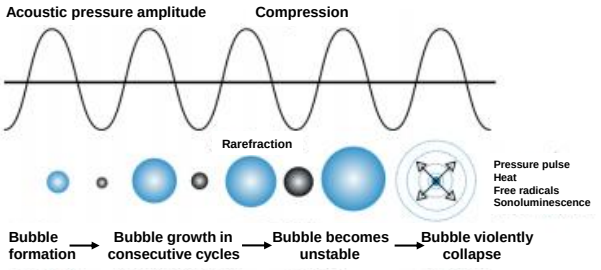

Fig. 9 A generalized view of bubble dynamics in an ultrasonic field [21].

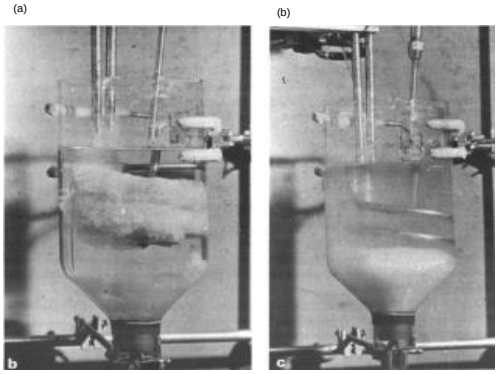

Fig. 10 Crystallization of potassium nitrate from a 28% aqueous solution: (a) Crystallization has ceased because of crusting on the coil, (b) Crystallization is proceeding with incrustation prevented by ultrasonic vibration of the coil [22].

5. RESULTS AND DISCUSSION

The full-scale concentric reducer was numerically modeled in this study as shown in Fig. 11. The rate of contraction of the cross-section area of the reducer along its axis was not uniform. The stream-wise and cross-stream components of the instantaneous velocities were measured along several sections through: A-A to G-G as shown in Fig. 12.

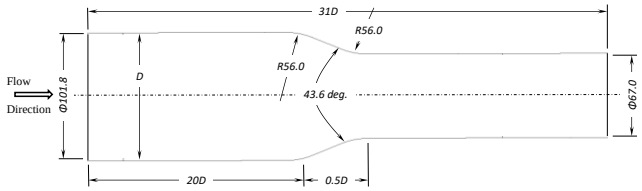

Fig. 11 Schematic diagram of a full-scale concentric reducer.

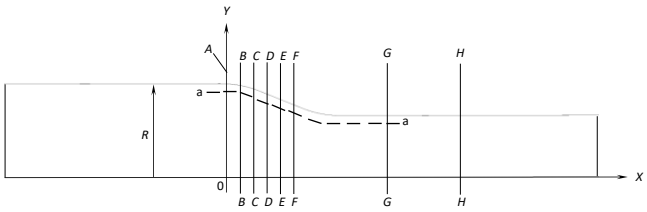

Fig. 12 Positions of sections where the stream-wise and cross-stream velocity components were measured.

The governing equations being solved in Reynolds stress model (RSM) are continuity, momentum and turbulence equations by commercial CFD code ANSYS fluent version 15.0. For an incompressible fluid, the equations of continuity and momentum balance for the mean motion are given as

$$\frac{\partial \overline{u}_i}{\partial x_i} = 0 \tag{4}$$

$$\frac{\partial \overline{u}_i}{\partial t} + \overline{u}_j \frac{\partial \overline{u}_i}{\partial x_j} = -\frac{1}{\rho}\frac{\partial \overline{p}}{\partial x_i} + \nu \frac{\partial^2 \overline{u}_i}{\partial x_j \partial x_j} - \frac{\partial}{\partial x_j} R_{ij} \tag{5}$$

where $R_{ij} = \overline{u_i' u_j'}$ is the Reynolds stress tensor and $u_i' = u_i - \overline{u}_i$

The Reynolds stress model (RSM) involves calculation of the individual turbulence stresses via a differential transport equation given as

$$\underbrace{\frac{\partial}{\partial t} R_{ij} + \overline{u}_k \frac{\partial}{\partial x_j} R_{ij}}_{\text{convective transport}} = \underbrace{+\frac{\partial}{\partial x_k}\left(\frac{\nu_t}{\sigma^k}\frac{\partial}{\partial x_k} R_{ij}\right)}_{\text{diffusive transport}} \underbrace{-\left[\overline{u_i' u_k'}\frac{\partial \overline{u}_j}{\partial x_k} + \overline{u_j' u_k'}\frac{\partial \overline{u}_i}{\partial x_k}\right]}_{P_{ij}=\text{production}} \tag{6}$$

$$\underbrace{-C_1 \frac{\varepsilon}{\kappa}\left[R_{ij} - \frac{2}{3}\delta_{ij}\kappa\right] - C_2\left[P_{ij} - \frac{2}{3}\delta_{ij}P\right]}_{\phi_{ij}=\text{pressure strain}} - \underbrace{\frac{2}{3}\delta_{ij}\varepsilon}_{\varepsilon_{ij}=\text{dissipation}}$$

where the production is given as

$$P_{ij} = -\overline{u_i' u_k'}\frac{\partial \overline{u}_j}{\partial x_k} - \overline{u_j' u_k'}\frac{\partial \overline{u}_i}{\partial x_k}, \quad P = \frac{1}{2}P_{ii} \tag{7}$$

Here, $\sigma^k = 1.0$, $C_1 = 1.8$ and $C_2 = 0.52$ are empirical constants $\kappa = \frac{1}{2}\overline{u_i' u_j'}$

The turbulence dissipation rate ε, is computed by the governing equation:

$$\frac{\partial \varepsilon}{\partial t}+\bar{u}_j\frac{\partial \varepsilon}{\partial x_j}=\frac{\partial}{\partial x_j}\left[\left(\nu+\frac{\nu_t}{\sigma^{\varepsilon}}\frac{\partial \varepsilon}{\partial x_j}\right)\right]-C_{\varepsilon 1}\frac{\varepsilon}{\kappa}R_{ij}\frac{\partial \bar{u}_i}{\partial x_j}-C_{\varepsilon 2}\frac{\varepsilon^2}{\kappa} \quad (8)$$

The values of the constants are given as,

$\sigma^{\varepsilon}=1.3, \quad C_{\varepsilon 1}=1.44, \quad C_{\varepsilon 2}=1.92$

The governing equations were discretised by using the vertex-centered finite volume method. The second-order central differencing scheme was applied for the spatial derivatives of pressure term and second-order upwind scheme was used for momentum term. The specific dissipation rate and Reynolds stresses were discretised by first-order upwind scheme. Pressure-velocity coupling was preserved by using the Coupled algorithm.

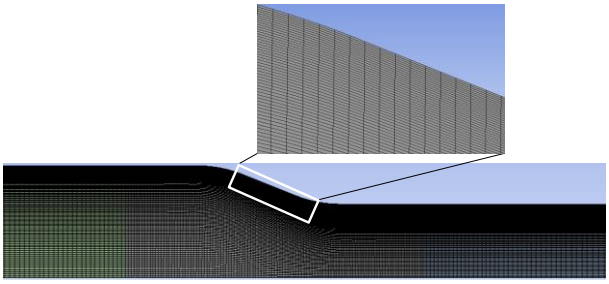

Fig. 13 Quadrilateral mesh on symmetric concentric reducer.

The preprocessor Design Modeller was used to generate two-dimensional Cartesian grid. The computational domain was discretised using quadrilateral structured meshes. Fine cells were used near the reducer wall whereas coarser cells were adopted around the centre of reducer as shown in Fig. 13. The mesh point distributions were concentrated near the reducer wall in order to give more accurate boundary-layer solution. The turbulent intensity at inlet of 5% and a uniform velocity distribution U_0 was defined at the inlet (0.268 m/s and 0.432 m/s, respectively). All velocity components were gradient-free for streamwise direction at the outlet. Pseudo transient explicit relaxation factors 0.5 for pressure, 0.5 for momentum, 1 for density and 0.75 for specific dissipation rate were considered. The convergence criterion for all the parameters was set on the order of 10^{-5}.

The variation of turbulent kinetic energy along the radius of the reducer was measured for Reynolds number of 27,130 as shown in Fig. 14. The variation in the turbulent kinetic energy supports the variation in the fluctuating velocity component.

The variation of both stream-wise (u'_x) and cross-stream (u'_r) velocity fluctuating components along the reducer model were measured at a distance of 0.08R from its wall as shown in Fig. 15. It is ascertained that the increase of cross-stream fluctuating velocity component in the reducer has a strong influence to promote scale growth on the wall.

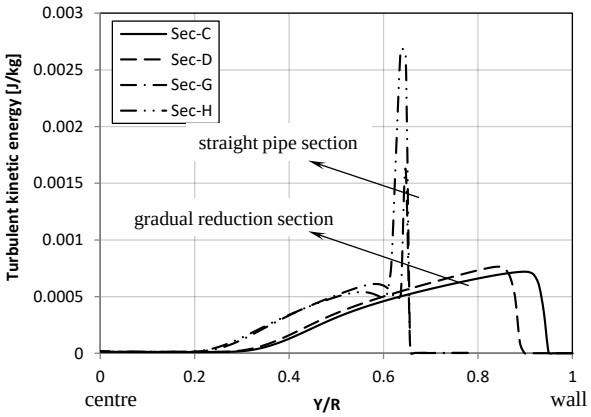

Fig. 14 The variation of the turbulent kinetic energy along the radius of the reducer: at the wall Y=R and Y/R=1, at the centre Y = 0 and Y/R = 0. The data were measured at the four different cross-section at Re = 27,130.

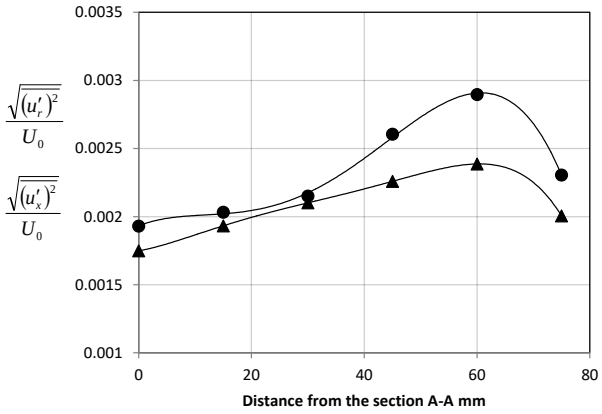

Fig. 15 Variations of normalised fluctuating components $\sqrt{\overline{(u'_r)^2}}\,/U_0$ (●) and $\sqrt{\overline{(u'_x)^2}}\,/U_0$ (▲) along the X-axis at the distance of 0.08R from the internal surface of the reducer: Re = 27,130 and V=0.268 m/s (101.8 mmφ pipe).

6. CONCLUSION

Fluid dynamics play an important role in scale growth mechanism and its suppression. The cross-stream, u'_r fluctuating velocity component in the reducer is greater than the stream-wise u'_x fluctuating velocity component in the reducer; it is believed that this is one of the reasons for more particle deposition as well as more scale growth in the concentric reducer.

REFERENCES

[1] M. Wagterveld, “Effect of ultrasound on calcium carbonate crystallization”, PhD Thesis, Delft University of Technology, 2013.

[2] A. R. Hind, S. K. Bhargava and S. C. Grocott, “The surface chemistry of Bayer process solids: a review”, International Journal of Colloids and Surfaces A: Physicochemical and Engineering Aspects, Vol. 146, No. 1, pp. 359-374, 1999.

[3] T. A. Hoang, M. Ang and A. L. Rohl, “ Effects of process parameters on gypsum scale formation in Pipes”,

International journal of Chemical Engineering & Technology, vol. 34**,** no. 6, pp. 1003-1009, 2011.

[4] S. J., Nawrath, M. M. K. Khan and M. C. Welsh, "An experimental study of scale growth rate and flow velocity of a super-saturated caustic–aluminate solution", International Journal of Mineral Processing, Vol 80, No. 2-4, pp. 116-125, 2006.

[5] J. N. Watson, A. R. Gerson, J. Addai-Mensah and T. J. Soar, "Nucleation mechanism of gibbsite from Bayer liquors", Light Metals**,** pp. 167-172, 1998.

[6] S. Veesler and R. Boistelle, "About supersaturation and growth rates of hydrargillite $Al(OH)_3$ in alumina caustic solutions", Journal of Crystal Growth, Vol. 130**,** No. 3-4, pp. 411-415, 1993.

[7] G. P. Demopoulos, "Aqueous precipitation and crystallization for the production particulate solids with desired properties", Journal of Hydrometallurgy, Vol. 96**,** No. 3, pp. 199-214, 2009.

[8] T. R. Bott, "Aspects of crystallization fouling", Experimental Thermal and Fluid Science, Vol. 14, pp. 356-360, 1997.

[9] D. Q. Kern and R. E. Seaton, "A theoretical analysis of thermal surface fouling" British Chemical Engineering, Vol. 4, No. 5, pp. 258-262, 1956.

[10] M. Bohnet, "Fouling of heat transfer surfaces", Chemical Engineering & Technology, Vol. 10**,** pp. 113-125, 1987.

[11] B. Bansal and H. Muller-Steinhagen, "Crystallization fouling in plate heat exchangers", Journal of Heat Transfer, Vol. 115, pp. 584-591, 1993.

[12] A. V. Deev, T. Rasheed, M. C. Welsh, M. M. K. Khan and M. G. Rasul, "Measurement of instantaneous flow velocities in a concentric reducer using Particle Image Velocimetry: Study of scale deposition", Journal of Experimental Thermal and Fluid Science, Vol. 33**,** pp. 1003-1011, 2009.

[13] J. Wu, G. Lane, I. Livk, B. Nguyuen, L. Graham, D. Stegink and T. Davis, "Swirl flow agitation for scale suppression", International Journal of Mineral Processing, Vol. 112–113, pp. 19-29, 2012.

[14] F. Fahiminia, "Initial fouling rate and delay time studies of aqueous calcium sulphate scaling under sensible heating conditions", PhD theis, The University of British Columbia, Canada, 2007.

[15] Z. Amjad, "Calcium sulphate dihydrate (gypsum) scale formation on heat exchanger surfaces: the influence of scale inhibitors", Journal of Colloid Interface Science, Vol. 123, pp. 523-536, 1998.

[16] Q. Yang, Y. Liu, A. Gu and Z. Shen, "Investigation of induction period and morphology of CaCO3 fouling on heated surface", Chem. Eng. Sci., Vol. 57, pp. 921-931, 2002.

[17] L. Tianqing, S. Yuwen and X. Wang, "Formation and remove processes of calcium carbonate fouling", Mitigation and Heat Exchanger Fouling Conference, Banff, Canada, 1999.

[18] S. N. Kazi, G. G. Duffy and X. D. Chen, "Fouling and fouling mitigation on heated metal surfaces", Journal of Desalination, Vol. 288, pp. 126-134, 2012.

[19] S. N. Kazi, G. G. Duffy and X. D. Chen, "Mineral scale formation and mitigation on metals and a polymeric heat exchanger surface", Journal of Applied Thermal Engineering, Vol. 30, pp. 2236-2242, 2010.

[20] D. Stegnik, T. Davis and J. Wu, "Operating experience with improved precipitation agitation system", 11 AQW Proceeding, Perth, Australia, 2012.

[21] D. Heath, B. Sirok, M. Hocevar and B. Pecnik, "The use of the cavitation effect in the mitigation of $CaCO_3$ deposits", Journal of Mechanical Engineering, Vol. 59, No. 4, pp. 203-215, 2013.

[22] M. J. Ashley, "Preventing deposition on heat exchange surfaces with ultrasound", Ultrasonics, September 1974.